Microscopic calculation of inelastic proton scattering off ^{18}O, ^{10}Be, ^{12}Be, and ^{16}C to study neutron excitation in neutron-rich nuclei

Yoshiko Kanada-En'yo
Department of Physics, Kyoto University, Kyoto 606-8502, Japan

Kazuyuki Ogata
Research Center for Nuclear Physics (RCNP), Osaka University, Ibaraki 567-0047, Japan;
Department of Physics, Osaka City University, Osaka 558-8585, Japan;
and Nambu Yoichiro Institute of Theoretical and Experimental Physics (NITEP), Osaka City University, Osaka 558-8585, Japan

(Received 8 August 2019; revised manuscript received 17 November 2019; published 30 December 2019)

Microscopic coupled-channel calculations of inelastic proton scattering are performed to study neutron excitations in the 2^+_1 states of ^{18}O, ^{10}Be, ^{12}Be, and ^{16}C. The proton-nucleus potentials in the coupled-channel calculation are microscopically derived by folding the Melbourne *g*-matrix *NN* interaction with the matter and transition densities of the target nuclei obtained via structure model calculations of the antisymmetrized molecular dynamics. The calculated results reasonably reproduce the elastic and inelastic proton scattering cross section, and support the dominant contribution of neutrons in the 2^+_1 excitation of ^{12}Be and ^{16}C as well as ^{18}O. The sensitivity of the inelastic scattering cross sections to the neutron transition density is discussed as well as the exotic behavior of the neutron transition density with amplitude in the outer regions of ^{12}Be and ^{16}C.

DOI: 10.1103/PhysRevC.100.064616

I. INTRODUCTION

Shape differences in the proton and neutron matter distributions in nuclei are interesting phenomena in unstable nuclei. To explore the difference between the neutron and proton deformations (or collectivity), the neutron and proton transition matrix elements in the ground-band $2^+_1 \to 0^+_1$ transition have been investigated for a long time. In a naive expectation for ordinary nuclei with the same proton and neutron deformation, the ratio of the neutron transition matrix element (M_n) to the proton transition matrix element (M_p) should be N/Z. However, the relation $M_n/M_p \approx Z/N$ is not satisfied, even in stable nuclei with proton or neutron shell closure, as reported in Ref. [1]. For example, in ^{18}O and ^{48}Ca, this ratio becomes significantly larger than N/Z, which indicates neutron dominance in the 2^+_1 excitation due to proton shell closure. The phenomena of shape differences and/or neutron dominance have also been suggested to occur in unstable nuclei such as ^{10}Be, ^{12}Be, and ^{16}C [2–15].

Experimental information concerning the proton part M_p can be directly obtained from the $E2$ strength. Conversely, the determination of the neutron part (M_n) is not easy, even for stable nuclei. As indirect measurements, inelastic hadron scattering experiments have been performed using probes such as α, proton, neutron, and π^-/π^+. By combining the hadron scattering data with the electromagnetic data, M_n and M_p have been discussed based on reaction analyses (see Refs. [1,16] and references therein). For ^{18}O, the neutron matrix element of the $2^+_1 \to 0^+_1$ transition has been intensively investigated and an anomalously large value of $M_n/M_p \approx 2$ has been deduced from the inelastic scattering data [16–19], consistent with the $B(E2)$ of the mirror transitions of ^{18}Ne and ^{18}O [20].

In studies of unstable nuclei, the neutron collectivity, i.e., the M_n/M_p ratio, has been investigated extensively using inelastic proton scattering experiments. [3,7,9,12,21–32]. Cross sections of inelastic proton scattering off unstable nuclei are measured in inverse kinematics using radioactive ion beams on proton targets. However, experimental data for exotic nuclei are limited to a small range of scattering angles at one of a few incident energies and are not high quality in many cases except for very light unstable nuclei such as ^{6}He. Under the constraint that the available data are limited, reaction analyses may be influenced by model ambiguities. For example, proton-nucleus optical potentials can be more or less uncertain because the phenomenological tuning of the potential parameters requires precise data of the elastic scattering cross sections. Possible model ambiguity also arises from the structure part. Collective model transition densities, which are often adopted in reaction analyses, are no longer valid in nuclei far from the stability line or in light stable nuclei with cluster structures. When experimental information is unknown or limited, it is useful to apply a more microscopic framework that can systematically describe inelastic scattering off various nuclei without fine tuning the model parameters.

The *ab initio* approach [33,34] is one of the most suitable frameworks for this purpose. Despite great progress in the *ab initio* description of the nuclear structure and reactions, however, it is applicable to rather limited systems (small mass numbers). Further, such calculations are computationally demanding and their applicability to systematic research

is nontrivial. Alternatively, in the present study, we adopt a microscopic folding model (MFM) approach for the sake of flexibility. As one research milestone in this direction, the Melbourne group has demonstrated the success of MFM in reproducing cross sections and spin observables of proton-nucleus elastic scattering for a wide range of target mass numbers at incident energies from 65 to 200 MeV with no free adjustable parameters [35,36]. A striking feature of their work is that the imaginary part of the g-matrix interaction is also generated and directly employed in the MFM calculation. This is an advantage over other MFM studies in which the imaginary part of the effective nucleon-nucleon interaction is treated phenomenologically [37–39].

Triggered by this complete MFM calculation by the Melbourne group, a microscopic description of proton-nucleus [40–43] and α-nucleus [42,44] elastic scattering has been intensively developed. Very recently, this framework was successfully applied to α-nucleus inelastic processes [43,45–47]. In these studies, a simplified treatment of the exchange term of the optical potential, validated in Refs. [40,48] for nucleon-nucleus scattering above 65 MeV, was adopted. This simplification makes the union of the nuclear reaction and structure calculations easier because then only the nuclear one-body density is needed. Note that the MFM framework adopted in the present study is based on the multiple scattering theory (MST) by Kerman, McManus, and Thaler [49]. In Ref. [43], the applicability of the framework to nucleon-nucleus elastic scattering was examined for a wide range of incident energies. As described below, to treat the elastic and inelastic scatterings on the same footing, we expand the wave function of the reaction system by several eigenstates of the target nucleus. This indicates that the higher-order effects coming from the channels that have the asymptotics assumed in the MST are explicitly taken into account. Conversely, possible coupling effects from rearrangement and breakup channels are treated effectively within the accuracy of the MST.

In the structure part, we adopt antisymmetrized molecular dynamics (AMD), which is a structure model suitable for providing systematic inputs of nuclei with various structures. In particular, it is a powerful model for cluster states in unstable nuclei. Another merit of AMD is that it can directly examine the nuclear deformation effect on the matrix elements, M_p and M_n, using not the effective charges but the bare charges of the protons and neutrons. However, AMD sometimes has quantitative problems in fine reproductions of the electric transition properties measured by electric probes. To reduce the structure model ambiguity as much as possible, we renormalize the theoretical proton transition densities to fit the experimental $B(E2)$ if it exists. For $N \neq Z$ unstable nuclei, the neutron part of the structure input may contain ambiguities and should be tested against proton inelastic scattering data. ^{18}O is a special case of a $Z \neq N$ stable nucleus, for which detailed transition densities are available from experimental data of electron and proton inelastic scattering in normal kinematics [19]. These data are used to check the applicability of the present reaction model without structure model ambiguities.

In this paper, we investigate inelastic proton scattering to the 2^+_1 states of ^{18}O, ^{10}Be, ^{12}Be, and ^{16}C with coupled-channel (CC) calculations of the MFM using the Melbourne g-matrix effective NN interaction [35]. The proton and neutron matter and transition densities of the target nuclei are calculated using AMD [50–52]. As test cases, we first show applications to proton scattering off $Z = N$ nuclei, i.e., ^{12}C and ^{16}O. Then, we apply the same method to proton scattering off ^{18}O, ^{10}Be, ^{12}Be, and ^{16}C. The sensitivity of the 2^+_1 cross sections to M_n and M_p is analyzed while focusing on the neutron-proton difference in the transition densities of ^{12}Be and ^{16}C. Here, we emphasize that we include no adjustment parameters in the reaction calculations. Within the accuracy of MST, we therefore unambiguously relate the structure inputs to the scattering observables with a minimal task.

The paper is organized as follows. The next section describes the present framework of the microscopic coupled-channel (MCC) calculation and that of the structure calculations for target nuclei. Results for ^{12}C and ^{16}O are shown in Sec. III, and results and discussion for the $N \neq Z$ case of ^{18}O, ^{10}Be, ^{12}Be, and ^{16}C are given in Sec. IV. Finally, a summary is given in Sec. V.

II. METHOD

The present reaction calculation for proton scattering is the MCC calculation of the single-folding model. As inputs from the structure calculations, the target densities are calculated with AMD combined with and without the cluster model of the generator coordinate method (GCM). The AMD and AMD+GCM calculations of the target nuclei are the same as those of Refs. [4,46,47,53–55]. The definitions of the densities and form factors in the structure calculation are explained in Ref. [46]. For details, the reader is referred to those references.

A. Microscopic coupled-channel calculation

The diagonal and coupling potentials for the nucleon-nucleus system are microscopically calculated by folding the Melbourne g-matrix NN interaction [35] with the target densities described in Sec. II B. The Melbourne g matrix is obtained by solving a Bethe-Goldstone equation in uniform nuclear matter at a given incident energy; the Bonn B potential [56] is adopted as a bare NN interaction. In Ref. [35], the Melbourne g-matrix interaction was constructed and applied to a systematic investigation of proton elastic and inelastic scattering off various stable nuclei and some neutron-rich nuclei at energies from 40 to 300 MeV. The nonlocality arising from the exchange term was rigorously treated, and the central, spin-orbit, and tensor contributions were taken into account. As a result, it was clearly shown that microscopic calculations with the Melbourne g matrix for proton-nucleus scattering have predictive power for proton-nucleus elastic and inelastic cross sections and spin observables. Later, the framework was also applied to proton inelastic scattering off ^{10}C and ^{18}O [36].

In the present study, we adopt a simplified single-folding model described in Ref. [40]. We employ the Brieva and Rook (BR) prescription [57–59] to localize the exchange terms. The validity of the BR localization for nucleon-nucleus and nucleus-nucleus scattering has been confirmed

in Refs. [40,48] and Ref. [60], respectively. This simplified single-folding model has been successfully applied to nucleon-nucleus elastic scattering for various cases [40–43]. In this study, we extend this model to proton inelastic scattering in a manner similar to that in our recent studies on α inelastic scattering [46,47]. To avoid complexity, we only take into account the central part of the proton-nucleus potential. The spin-orbit interaction is known to smear the dip structure of the diffraction pattern in general. Even though at higher energies, say, above 150–200 MeV, it can also somewhat affect the absolute amplitudes near the peaks, such an effect is expected to be minor in the energy region considered in this study. As in previous studies, including that by the Melbourne group [35], the local density approximation is adopted to apply the g-matrix interaction to a finite nucleus.

The cross sections of the elastic and inelastic scattering are calculated via the CC calculations using the proton-nucleus potentials obtained with the AMD densities for ^{18}O, ^{10}Be, ^{12}Be, and ^{16}C, and the AMD+GCM densities for ^{12}C and ^{16}O. For ^{12}C, we also use the densities of a 3α-cluster model of the resonating group method (RGM) [61].

Note that a similar approach, an MCC calculation with the Jeukenne-Lejeune-Mahaux (JLM) interaction [62], has been applied to proton inelastic scattering off ^{10}Be and ^{12}Be in an earlier study by Takashina *et al.* [11]. It has also been used in continuum-discretized CC calculations for nucleon-induced breakup reactions of ^{6,7}Li [63–65] and ^{11}Li [66]. The JLM interaction is another type of g-matrix effective interaction that only has the direct term. This property allows one to implement it in reaction calculations with the minimal task. However, in general, phenomenological tuning of the JLM interaction is necessary to obtain the scattering data, though not in the present interaction.

B. Structure calculations for target nuclei

For the structure calculation of the target nuclei, we adopted the AMD wave functions obtained via the variation after projections (VAP). In the AMD+VAP method, the variation is performed for the spin-parity projected AMD wave function, as in Refs. [67,68]. The method was applied in the structure studies of ^{10}Be, ^{12}Be, and ^{16}C in Refs. [4,53,54]. In the present paper, the same method is applied to ^{18}O to obtain the wave functions of the 0^+_1 and 2^+_1 states. For ^{12}C and ^{16}O, the AMD+VAP method is combined with the 3α- and ^{12}C + α-cluster GCM, respectively, as in Refs. [46,47,55,69,70]. In this paper, we simply call the AMD+VAP method "AMD" and that with the cluster GCM "AMD+GCM."

The AMD wave functions used in this paper are, in principle, the same as those in Refs. [54,67]. We utilized the ^{10}Be wave function for ^{10}C by assuming mirror symmetry. For ^{16}C, the VAP(c) wave function of Ref. [4] was adopted. The wave functions and transition densities of ^{12}C and ^{16}O are consistent with those of AMD+GCM used for α scattering in Refs. [46,47].

The neutron and proton matter and transition densities are calculated with the AMD and AMD+GCM wave functions. We denote the neutron and proton transition densities as $\rho^{\rm tr}_n(r)$ and $\rho^{\rm tr}_p(r)$, respectively. For $N = Z$ nuclei (^{12}C and ^{16}O), half of the isoscalar density is used as the proton (neutron) density in the mirror symmetry assumption. For quantitative discussions of inelastic cross sections, we scale the original transition densities $\rho^{\text{tr-cal}}_p(r)$ to adjust the theoretical $B(E\lambda)$ values to the experimental data as

$$\rho^{\rm tr}_p(r) = \left(M^{\rm exp}_p/M^{\rm cal}_p\right)\rho^{\text{tr-cal}}_p(r). \tag{1}$$

Here, the rank λ ($\lambda > 0$) transition matrix elements for the neutron and proton parts are defined as

$$M_{n,p} \equiv \int r^{2+\lambda}\rho^{\rm tr}_{n,p}(r)dr \tag{2}$$

and are related to the transition strengths as

$$B^{(n),(p)}_{\lambda} = \frac{1}{2J_i+1}|M_{n.p}|^2, \tag{3}$$

where J_i is the angular momentum of the initial state. The $E2$ transition strength is given by the proton $\lambda = 2$ transition strength as $B(E2) = e^2B^{(p)}_{\lambda=2}$.

The adopted states in the CC calculations for ^{10}Be, ^{12}Be, ^{16}C, and ^{18}O are ^{10}Be($0^+_{1,2}$, $2^+_{1,2,3}$), ^{12}Be($0^+_{1,2}$, $2^+_{1,2}$), ^{16}C(0^+_1, $2^+_{1,2}$), and ^{18}O(0^+_1, 2^+_1), respectively. All $\lambda = 0$ and $\lambda = 2$ transitions between these states are taken into account. The experimental values of the excitation energies are adopted as inputs to the CC calculations.

In the CC calculations for ^{12}C and ^{16}O, all the inputs from the structure part, such as the adopted states, excitation energies, and transitions, are the same as those used for the α scattering with the AMD+GCM wave functions in Refs. [46,47].

As shown later, the CC effect makes only a minor contribution to the inelastic scattering to the 2^+_1 state at incident energies higher than 25 MeV and the cross sections are approximately described by the one-step process of the distorted wave Born approximation (DWBA).

III. RESULTS FOR ^{12}C AND ^{16}O

The 0^+_1 and 2^+_1 cross sections of ^{12}C at incident energies of $E_p = 35$, 65, and 135 MeV are shown in Fig. 1, and those of ^{16}O at $E_p = 35$ and 135 MeV are shown in Fig. 2. In addition to the CC calculation, the one-step cross sections obtained by the DWBA calculation are also shown. The small difference between the CC and DWBA cross sections indicates that the CC effect is minor.

The AMD+GCM result for ^{12}C was compared to experimental data and also to the calculation using the RGM density. From the electron scattering data, the RGM density is known to be of good quality and better than the AMD+GCM density [46,61]. As seen in Fig. 1, the present calculation with the AMD+GCM density reproduces the elastic proton scattering cross sections of ^{12}C at forward angles well but somewhat underestimates the third peak. A better result is obtained by the calculation with the RGM density, which is consistent with the findings of Ref. [43]. The inelastic proton scattering cross sections of ^{12}C(2^+_1) are described reasonably well with the AMD+GCM and RGM calculations except for the cross sections at $E_p = 35$ MeV. The RGM density again gives a better agreement with the data at large angles. This result

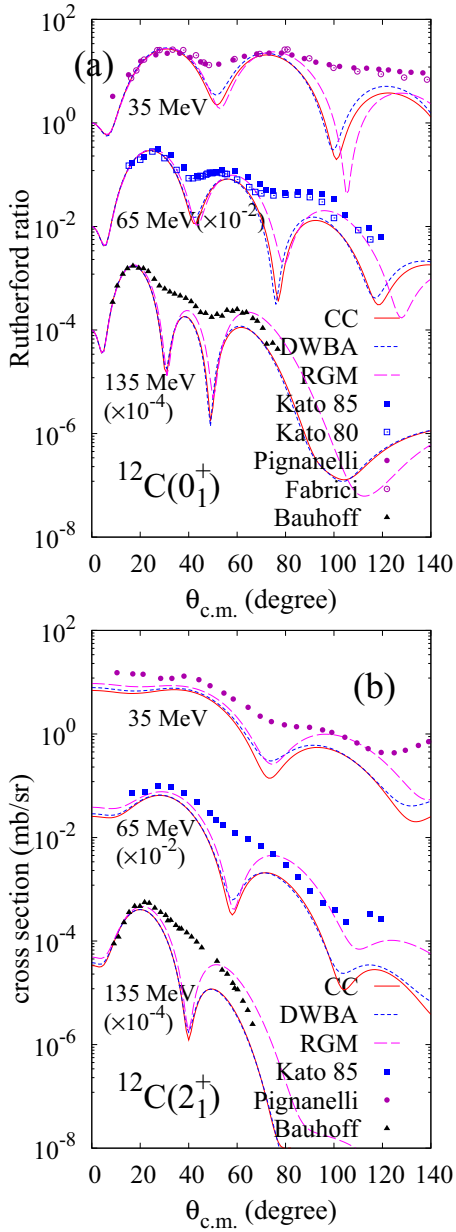

FIG. 1. Cross sections of the elastic and inelastic proton scattering off ^{12}C at $E_p = 35$ MeV, $E_p = 65$ MeV ($\times 10^{-2}$), and $E_p = 135$ MeV ($\times 10^{-4}$) calculated using the AMG+GCM and RGM densities. The results of the CC and DWBA calculations with the AMD+GCM densities and the CC calculation with the RGM densities are shown by the red solid, blue dotted, and magenta dashed lines, respectively. The experimental data are from Refs. [71–75].

indicates that the quality of the structure model densities can be tested using detailed proton scattering data. For the proton scattering off ^{16}O, the present calculation reproduces the elastic and inelastic cross sections well (Fig. 2). Note that the 2^+_1 state of ^{16}O is not the ground-band member but belongs to the $^{12}\mathrm{C} + \alpha$-cluster band built on the 0^+_2 state. The present microscopic approach works well even for such a developed cluster state with a structure very different from the ground state.

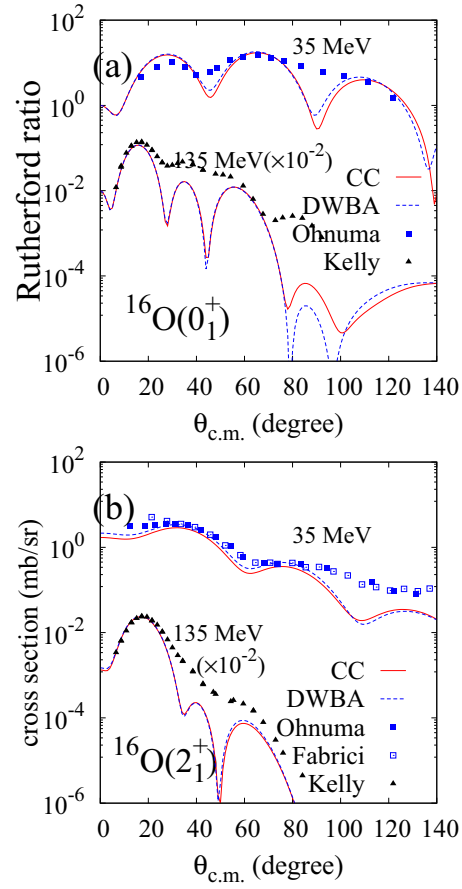

FIG. 2. Cross sections of the elastic and inelastic proton scattering off ^{16}O at $E_p = 35$ MeV and $E_p = 135$ MeV ($\times 10^{-2}$) calculated using the AMG+GCM densities. The results of the CC and DWBA calculations are shown by the red solid and blue dotted lines, respectively. The experimental data are from Refs. [71,76,77].

IV. RESULTS FOR $Z \neq N$ NUCLEI

A. Structural properties

The theoretical and experimental values of structural properties of the target nuclei are listed in Tables I and II. The energies are shown in Table I, and the radii and $\lambda = 2$ transition strengths, as well as the M_n/M_p ratio, are shown in Table II. The structure calculations of ^{10}Be, ^{12}Be, and ^{16}C are consistent with Refs. [4,53,54].

B. Results for ^{18}O

In the $2^+_1 \to 0^+_1$ transition of ^{18}O, the significant $B^{(p)}_{\lambda=2}$ is experimentally known but is significantly underestimated by the AMD calculation meaning that the proton excitation from the p-shell closure is not sufficiently described in the theory. For the neutron part, the large $B^{(n)}_{\lambda=2}$ of the AMD calculation indicates neutron dominance, which is qualitatively consistent with the mirror transition of ^{18}Ne [20] and the proton scattering experiment [19].

The calculated densities and form factors of ^{18}O are shown in Figs. 3 and 4, respectively, together with the data measured by the electron scattering experiments. Here the theoretical

TABLE I. Binding and excitation energies of ^{18}O, ^{10}Be, ^{12}Be, and ^{16}C. The theoretical values of ^{10}Be, ^{12}Be, and ^{16}C are from Refs. [4,53,54], and the experimental values are from Refs. [78–81]. The band assignment (K^π) is given based on the AMD calculation.

		Energy (MeV)	
	Band	AMD	Exp.
^{18}O(0^+_1)	$K=0^+_1$	131.1	139.80
^{18}O(2^+_1)	$K=0^+_1$	2.0	1.98
^{10}Be(0^+_1)	$K=0^+_1$	61.1	64.98
^{10}Be(2^+_1)	$K=0^+_1$	2.7	3.37
^{10}Be(2^+_2)	$K=2^+$	6.8	5.96
^{10}Be(0^+_2)	$K=0^+_2$	7.8	6.179
^{10}Be(2^+_3)	$K=0^+_2$	9.0	7.54
^{12}Be(0^+_1)	$K=0^+_1$	61.9	68.65
^{12}Be(2^+_1)	$K=0^+_1$	1.8	2.11
^{12}Be(0^+_2)	$K=0^+_2$	3.6	2.251
^{12}Be(2^+_2)	$K=0^+_2$	4.6	
^{16}C(0^+_1)	$K=0^+_1$	102.6	110.75
^{16}C(2^+_1)	$K=0^+_1$	2.4	1.77
^{16}C(2^+_2)	$K=2^+$	7.8	3.99

proton transition density $\rho_p^{\text{tr-cal}}(r)$ and form factors $F^{\text{cal}}(q)$ are scaled by the factor $M_p^{\text{exp}}/M_p^{\text{cal}} = 3.88$ such that $\rho_p^{\text{tr}}(r) = (M_p^{\text{exp}}/M_p^{\text{cal}})\rho_p^{\text{tr-cal}}(r)$ and $F(q) = (M_p^{\text{exp}}/M_p^{\text{cal}})F^{\text{cal}}(q)$ so as to fit the experimental $B(E2)$ value. After the scaling, the experimental data are reproduced well except in the small r (large q) region.

For the neutron transition density $\rho_n^{\text{tr}}(r)$ of ^{18}O, we tentatively assume mirror symmetry and scale $\rho_n^{\text{tr-cal}}(r)$ with the scaling factor $M_p^{\text{exp}}(^{18}\text{Ne})/M_n^{\text{cal}} = 1.72$ to prepare the default input $\rho_n^{\text{tr}}(r)$ in the reaction calculation. However, if we take into account mirror symmetry breaking, another choice may be possible; for example, an approximately 10% smaller value than $M_p^{\text{exp}}(^{18}\text{Ne})$ was theoretically recommended for $M_n(^{18}\text{O})$ in Ref. [19]. In Figs. 3(b) and 3(c), the default $\rho_n^{\text{tr}}(r)$ is compared to the experimental estimation [denoted $\rho_{n,\text{exp}}^{\text{tr}(p,p')}(r)$] in Ref. [19], which was reduced from inelastic proton scattering at $E = 135$ MeV/u via a model analysis. $\rho_{n,\text{exp}}^{\text{tr}(p,p')}(r)$ gives $B^{(n)}_{\lambda=2} = 38$ fm^4, which is slightly smaller than the $B^{(n)}_{\lambda=2} = 50$ fm^4 of $\rho_n^{\text{tr}}(r)$ adjusted to $B(E2;\,^{18}\text{Ne})$. The 12% reduced transition density [$0.88\rho_n^{\text{tr}}(r)$] gives the same strength ($B^{(n)}_{\lambda=2} = 38$ fm^4) as $\rho_{n,\text{exp}}^{\text{tr}(p,p')}(r)$ but shows a different radial behavior compared to $\rho_{n,\text{exp}}^{\text{tr}(p,p')}(r)$. Compared to the theoretical transition density, $\rho_{n,\text{exp}}^{\text{tr}(p,p')}(r)$ has a smaller amplitude at the nuclear surface ($r = 3$–4 fm) and an enhanced outer tail in the $r \gtrsim 5$ fm region [see Fig. 3(c)]. In the reaction analysis, we consider this difference between $\rho_{n,\text{exp}}^{\text{tr}(p,p')}(r)$ and the default $\rho_n^{\text{tr}}(r)$ as a model ambiguity arising from the neutron transition density.

We calculated the cross sections of the proton scattering at $E = 24.5$, 35, 43, and 135 MeV/u, and those of the neutron scattering at $E = 24$ MeV/u. These cross sections were compared to the experimental data. The results are shown in Figs. 5 and 6. The calculation reproduces the elastic and inelastic proton scattering cross sections reasonably well over a wide range of energies, i.e., $E = 24$–135 MeV/u. It also reproduces the neutron scattering cross sections at $E = 24$ MeV/u well. In comparison to the DWBA calculation shown in Fig. 7, one can see that the CC effect is minor in the 2^+_1 cross sections.

Let us discuss the ambiguity arising from the proton and neutron transition densities. As shown previously, the (scaled) proton part $\rho_p^{\text{tr}}(r)$ used in the present calculation reproduces the experimental data measured by the electron scattering well, whereas the neutron part $\rho_n^{\text{tr}}(r)$ has different r behavior from the experimental one $\rho_{n,\text{exp}}^{\text{tr}(p,p')}(r)$. To see the effect of this

TABLE II. Matter, proton, and neutron radii, and transition strengths of ^{18}O, ^{10}Be, ^{12}Be, and ^{16}C. The theoretical values of the AMD calculation for ^{10}Be, ^{12}Be, and ^{16}C are from Refs. [4,53,54], and the experimental values are from Refs. [78–81]. The data of $B^{(p)}_{\lambda=2} = B(E2)/e^2$ for ^{16}C are the values reported in Refs. [13,82]. The experimental values of $B(E2)/e^2$ for the mirror nuclei (^{18}Ne and ^{10}C) are shown for $B^{(n)}_{\lambda=2}$ for ^{18}O and ^{10}Be (labeled $^{*\text{mir}}$).

	R_p (fm)	R_n (fm)	R_m (fm)
^{18}O(0^+_1)	2.75	2.88	2.82
Exp.	2.62	2.83$^{*\text{mir}}$	2.61(8)
	$B^{(p)}_{\lambda=2}$ (fm^4)	$B^{(n)}_{\lambda=2}$ (fm^4)	M_n/M_p
^{18}O($2^+_1 \to 0^+_1$)	0.7	18.6	5.4
Exp.	9.3(3)	50(5)$^{*\text{mir}}$	2.3(2)$^{*\text{mir}}$
	R_p (fm)	R_n (fm)	R_m (fm)
^{10}Be(0^+_1)	2.50	2.56	2.54
Exp.	2.17		2.30(2)
	$B^{(p)}_{\lambda=2}$ (fm^4)	$B^{(n)}_{\lambda=2}$ (fm^4)	M_n/M_p
^{10}Be($2^+_1 \to 0^+_1$)	11.6	8.9	0.9
Exp.	10.2(1.0)	12.2(1.9)$^{*\text{mir}}$	1.1(1)$^{*\text{mir}}$
^{10}Be($2^+_2 \to 0^+_1$)	0.2	3.2	3.9
^{10}Be($2^+_3 \to 0^+_1$)	0.1	0.7	2.5
^{10}Be($2^+_3 \to 0^+_2$)	34.5	118	1.8
	R_p (fm)	R_n (fm)	R_m (fm)
^{12}Be(0^+_1)	2.67	2.94	2.85
Exp.	2.39		2.59(6)
^{12}Be(0^+_2)	2.56	2.84	2.75
	$B^{(p)}_{\lambda=2}$ (fm^4)	$B^{(n)}_{\lambda=2}$ (fm^4)	M_n/M_p
^{12}Be($2^+_1 \to 0^+_1$)	14.4	51.1	1.9
Exp.	14.2(2.8)		
^{12}Be($2^+_2 \to 0^+_1$)	0.0	7.4	25.4
^{12}Be($2^+_2 \to 0^+_2$)	7.5	9.0	1.1
	R_p (fm)	R_n (fm)	R_m (fm)
^{16}C(0^+_1)	2.58	2.85	2.75
Exp.			2.70(3)
	$B^{(p)}_{\lambda=2}$ (fm^4)	$B^{(n)}_{\lambda=2}$ (fm^4)	M_n/M_p
^{16}C($2^+_1 \to 0^+_1$)	2.7	27.0	3.2
Exp. [82]	2.6(9)		
Exp. [13]	4.15(73)		
^{16}C($2^+_2 \to 0^+_1$)	2.6	0.1	0.2

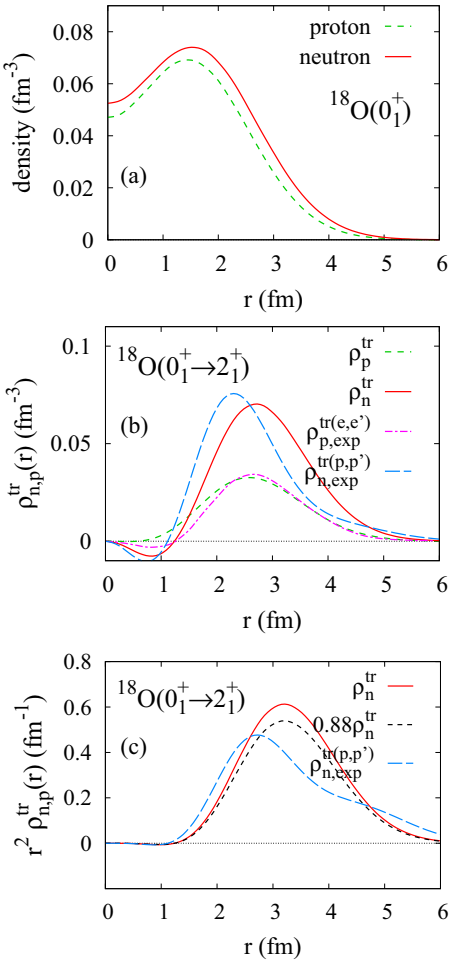

FIG. 3. Neutron and proton densities of ^{18}O: (a) the neutron and proton matter densities of the ground state, (b) the neutron and proton transition densities for the $0^+_1 \to 2^+_1$ transition, and (c) the r^2-weighted neutron transition density calculated with AMD. The renormalized proton and neutron transition densities adjusted to the experimental $B(E2)$ of ^{18}O and that of ^{18}Ne are shown, respectively. The experimental neutron transition density $\rho^{tr(p,p')}_{n,exp}$ reduced from the (p, p') scattering at $E = 135$ MeV/u [19] and the experimental proton transition density $\rho^{tr(e,e')}_{p,exp}$ measured with the electron scattering data [83] are also shown.

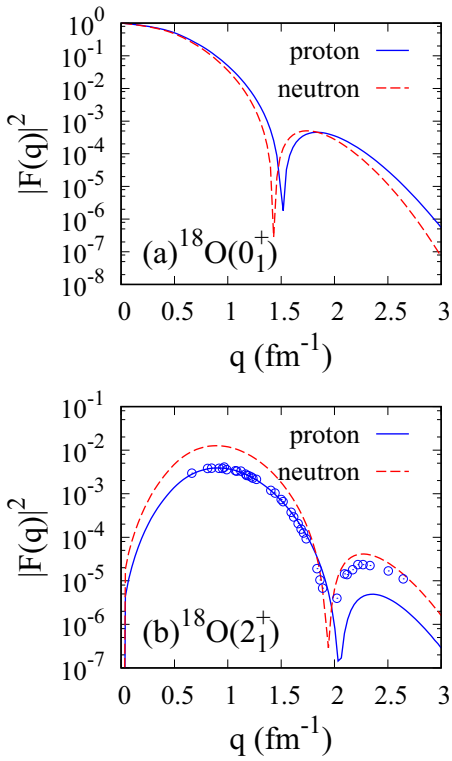

FIG. 4. Elastic and inelastic form factors of ^{18}O. The inelastic form factors for $0^+_1 \to 2^+$ are the renormalized ones adjusted to the experimental $B(E\lambda)$. The experimental data measured by the electron scattering are from Ref. [83].

difference in the neutron transition density on the inelastic cross sections, we performed the same reaction calculation using $\rho^{tr(p,p')}_{n,exp}(r)$ and $0.88\rho^{tr}_n(r)$. Figures 5(b) and 6(b) show the proton and neutron scattering cross sections obtained with $\rho^{tr(p,p')}_{n,exp}(r)$ (light-blue dashed lines) and $0.88\rho^{tr}_n(r)$ (blue dotted lines) in comparison to the default calculation (red solid lines) and experimental data. In the result of proton scattering with $\rho^{tr(p,p')}_{n,exp}(r)$, the cross sections at forward angles slightly decrease to 70% of the default calculation, and the second and third peaks at large angles are reduced further to 40–60% of the default calculation. The reduction rate at large angels is larger than the naive expectation of $38/50 \approx 75\%$ from the $B^{(n)}_{\lambda=2}$ ratio. This means that the outer tail amplitude of the neutron transition density makes a relatively minor contribution to the proton scattering cross sections compared to the surface amplitude even though it significantly enhances M_n, i.e., $B^{(n)}_{\lambda=2}$. The calculation with $\rho^{tr(p,p')}_{n,exp}(r)$ obtains better agreement with the proton scattering data at least at $E = 24.5$ and 35 MeV/u suggesting that $\rho^{tr(p,p')}_{n,exp}(r)$ may be more appropriate than the default $\rho^{tr}_n(r)$ used in the present calculation. This indicates that proton scattering is a sensitive probe for the neutron transition density. In contrast to proton scattering, the neutron scattering cross sections are not very sensitive to the difference in the neutron transition densities, as expected from weaker *nn* interactions than *pn* interactions.

C. Results for ^{10}Be, ^{12}Be, and ^{16}C

Structure studies of ^{10}Be, ^{12}Be, and ^{16}C with AMD have been conducted in Refs. [4,53,54]. Here, we briefly describe the structural properties, in particular, of the ground bands in these nuclei.

In ^{10}Be, the $M_n/M_p = 0.9$ of the ground-band transition $2^+_1 \to 0^+_1$ in the AMD calculation is smaller than the $N/Z = 1.5$ naively expected from the collective model and in reasonable agreement with the experimental value ($M_n/M_p = 1.1$) reduced from the $B(E2)$ of the mirror transitions. This indicates that the neutron excitation is somewhat suppressed compared to the proton excitation in the 2^+_1 state. In addition to the 2^+_1 state of the ground $K^\pi = 0^+$ band, the 2^+_2 state of the side band ($K^\pi = 2^+$) is obtained due to the triaxial deformation. In the higher energy region, a second $K^\pi = 0^+$ band with a developed cluster structure appears.

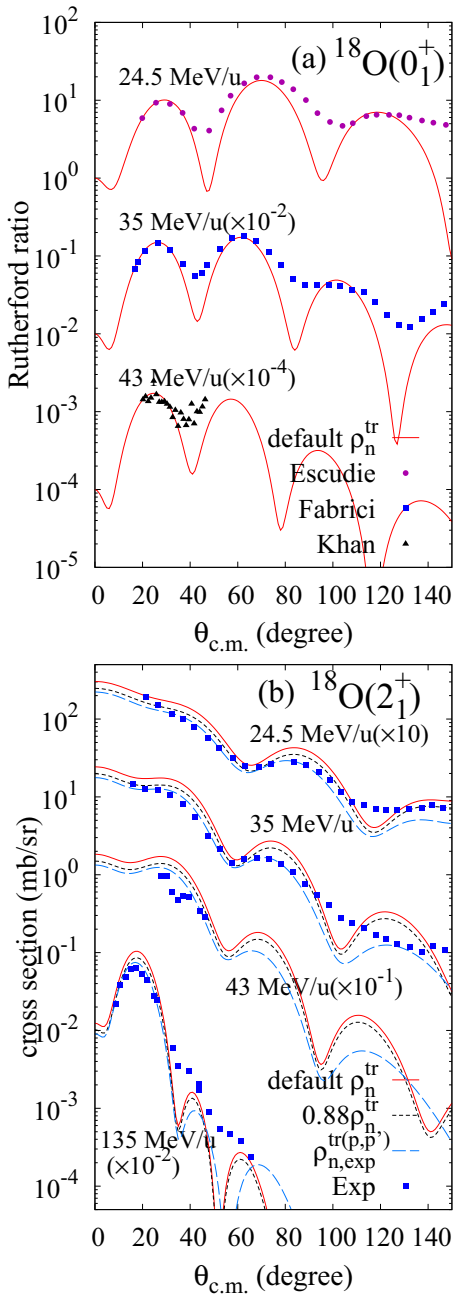

FIG. 5. Cross sections of the elastic and inelastic proton scattering off ^{18}O at $E = 24$ MeV/u (×10), 35 MeV/u, 43 MeV/u ($\times 10^{-1}$), and 135 MeV/u ($\times 10^{-2}$) calculated using the default AMD densities (solid lines). The experimental data for $E = 43$ MeV/u are the cross sections measured in inverse kinematics. For the 2^+_1 cross sections, the calculated result with the experimental neutron transition density $\rho_{n,\mathrm{exp}}^{\mathrm{tr}(p,p')}(r)$ and that with the reduced neutron transition density $0.88\rho_n^{\mathrm{tr}}(r)$ are also shown by the dashed and dotted lines, respectively. The experimental data are from Refs. [19,21,71,84].

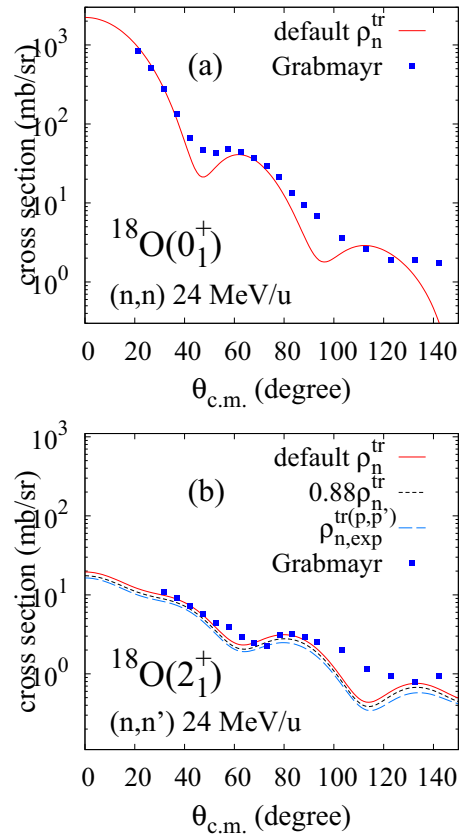

FIG. 6. Cross sections of (a) elastic and (b) inelastic neutron scattering off ^{18}O at $E = 24$ MeV/u. For the 2^+_1 cross sections, the CC calculation with the experimental neutron transition density $\rho_{n,\mathrm{exp}}^{\mathrm{tr}(p,p')}(r)$ and that with $0.88\rho_n^{\mathrm{tr}}(r)$ are also shown by the blue dotted and light-blue dashed lines, respectively, in addition to that with the default AMD densities (the red solid lines). The data are from Ref. [18].

In ^{12}Be, the breaking of $N = 8$ magicity is known in the ground state from various experimental observations such as the Gamov-Tellar transitions, inelastic scattering, and knock-out reactions [3,88–92]. The AMD calculation obtains the largely deformed ground band ($K^\pi = 0^+_1$) with the dominant neutron $2\hbar\omega$ component. The ground-band transition, $2^+_1 \to 0^+_1$, is strong due to the large deformation compared to the weaker transition in the $K^\pi = 0^+_2$ band, which corresponds to the normal neutron p-shell closed configuration. In particular, the neutron transition is very strong due to the contribution of the two sd-orbit neutrons. The value of the ratio $M_n/M_p = 1.9$ ($M_n/M_p = 1.1$) was obtained for the $K^\pi = 0^+_1$ ($K^\pi = 0^+_2$) band. The ratio of the ground band is as large as $N/Z = 2$ due to the breaking of the $N = 8$ magicity.

In the case of ^{16}C, the AMD calculation predicted the weak proton transition in $2^+_1 \to 0^+_1$ due to the $Z = 6$ subshell closure. The observed $B(E2)$ values are consistent with this prediction. Conversely, the neutron transition is very large due to the contribution of the sd-orbit neutrons and results in the much larger ratio of $M_n/M_p = 3.2$ compared to $N/Z = 1.67$, i.e., the dominant neutron contribution in the ground-band transition.

Figures 8 and 9 show the neutron and proton matter densities of the ground state and the neutron and proton transition densities of the $2^+_1 \to 0^+_1$ transition of ^{10}Be, ^{12}Be, and ^{16}C. In ^{10}Be, the proton and neutron transition densities have peak amplitudes at the same position at the nuclear surface and

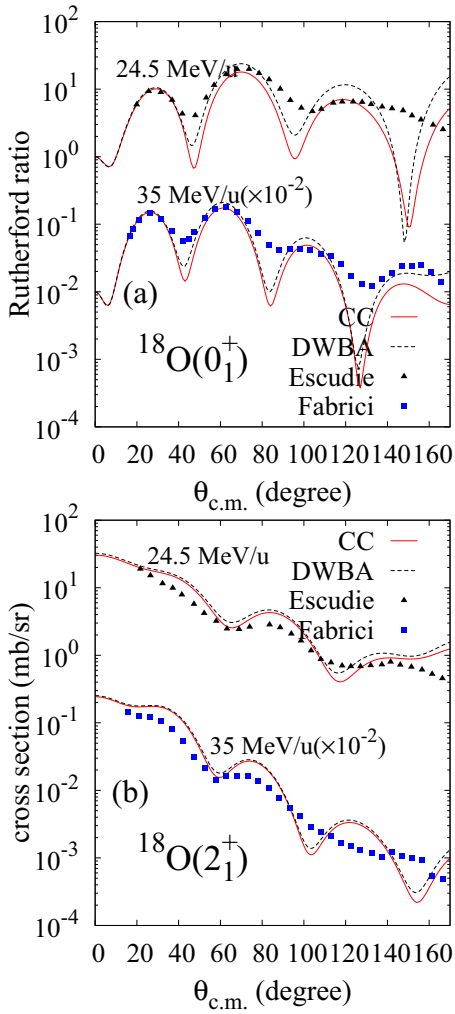

FIG. 7. Comparison of the CC and DWBA calculations of the proton scattering off ^{18}O with the default $\rho_n^{\rm tr}(r)$. The (a) elastic and (b) inelastic cross sections at $E = 24.5$ MeV/u and 35 MeV/u are shown in comparison to the experimental data [71,84].

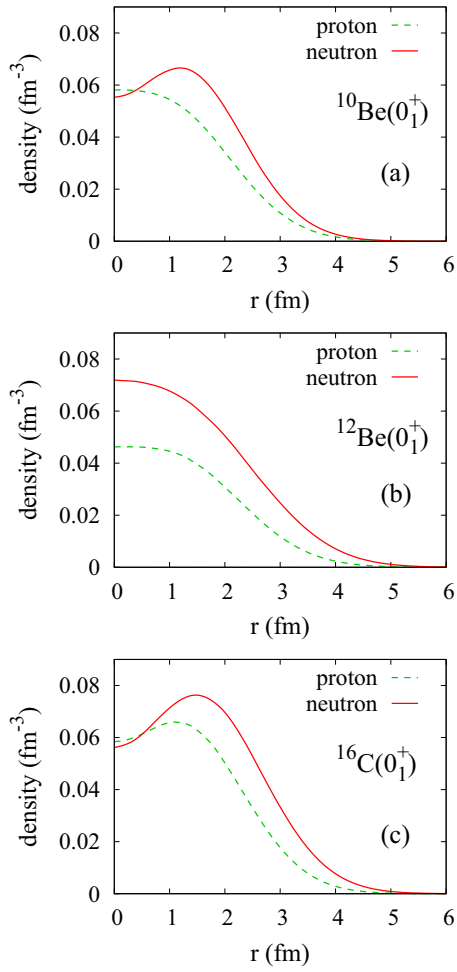

FIG. 8. Neutron and proton matter densities of the ground states of (a) ^{10}Be, (b) ^{12}Be, and (c) ^{16}C calculated with AMD.

approximately satisfy the relation $\rho_n^{\rm tr}(r) = (M_n/M_p)\rho_p^{\rm tr}(r)$. By contrast, for ^{12}Be and ^{16}C, the neutron transition density shows r behavior that is very different from the proton transition density. It has a peak amplitude in the $r \approx 3$ fm region much further out compared to the proton transition density due to the contribution of the sd-orbit neutrons and no longer satisfies the relation $\rho_n^{\rm tr}(r) = (M_n/M_p)\rho_p^{\rm tr}(r)$. This is different from the case of ^{10}Be, where the protons and neutrons in the same p shell contribute to the 2_1^+ excitation.

The proton scattering cross sections were calculated using the AMD densities. For ^{10}Be, the theoretical proton and neutron transition densities are renormalized to fit the experimental transition strengths ($B_{\lambda=2}^{(p),(n)}$) by the scaling factors $M_{p,n}^{\rm exp}/M_{p,n}^{\rm cal}$ listed in Table II. For ^{12}Be and ^{16}C, we use the original AMD transition densities, which reproduce the experimental $B(E2)$ values well. The calculated elastic and inelastic cross sections of ^{10}Be at $E = 60$ MeV/u, ^{12}Be at $E = 55$ MeV/u, and ^{10}C at $E = 45$ MeV/u are shown in Figs. 10 and 11. They are compared to the experimental data measured in inverse kinematics. In Fig. 12, the calculated cross sections of ^{16}C at $E = 33$ MeV/u are compared to the experimental data. The present calculation reproduces well the absolute amplitude of the 2_1^+ cross sections as well as the elastic cross sections.

In Fig. 11(b) for ^{12}Be, the DWBA calculation with the neutron transition density $\rho_n^{\rm tr}(r) = (M_n/M_p)\rho_p^{\rm tr}(r)$ is also shown. This calculation corresponds to the case with the collective model transition density. Compared to the result using the original AMD transition density, the cross sections somewhat increase and the peak and dip positions slightly shift toward larger angles.

For the neutron transition in ^{12}Be and ^{16}C, there are no data from the mirror nuclei. The good reproduction of the inelastic cross sections supports the reliability of the neutron transition densities adopted in the present calculation, that is, the dominant neutron contributions of $M_n/M_p \approx 2$ and $M_n/M_p \approx 3$ for ^{12}Be and ^{16}C, respectively. This result is qualitatively consistent with those in Refs. [9,11]. Note that that phenomenological adjustment parameters were needed in the reaction models of Refs. [9,11] but not in the present

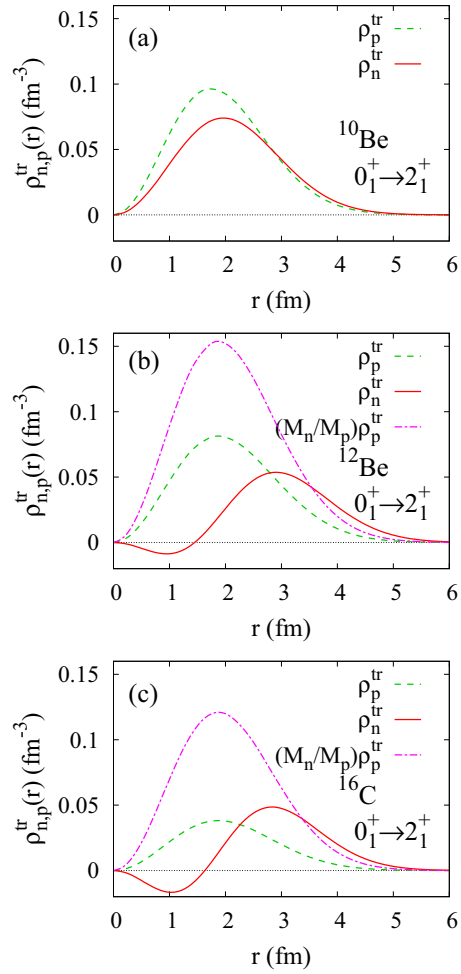

FIG. 9. Neutron ($\rho_n^{\rm tr}$) and proton ($\rho_p^{\rm tr}$) transition densities for $0_1^+ \to 2_1^+$ for (a) ^{10}Be, (b) ^{12}Be, and (c) ^{16}C calculated with AMD. The proton and neutron transition densities of ^{10}Be are renormalized to adjust the experimental $B(E2)$ values of ^{10}Be and ^{10}C, respectively.

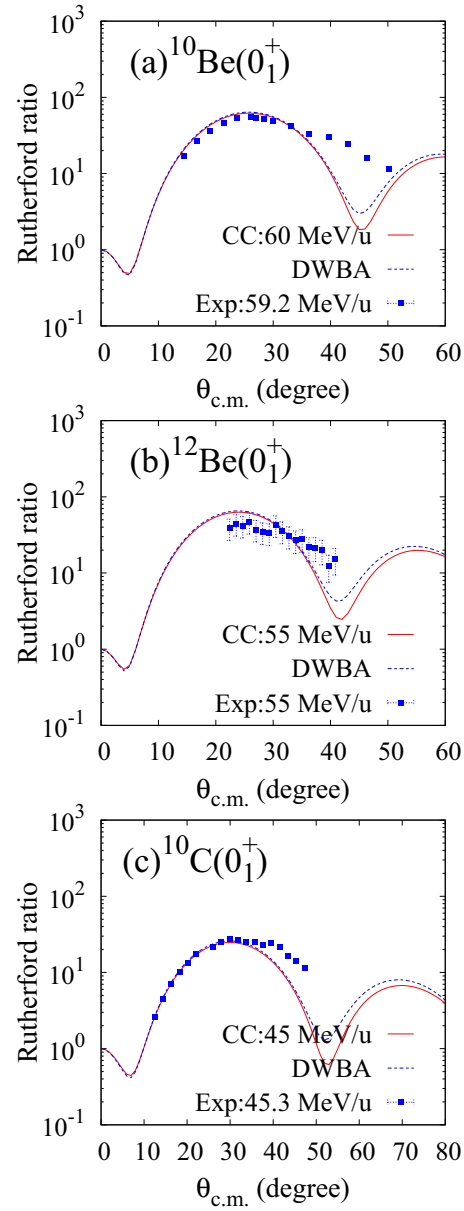

FIG. 10. Cross sections of elastic proton scattering off (a) ^{10}Be at $E = 60$ MeV/u, (b) ^{12}Be at $E = 55$ MeV/u, and (c) ^{10}C at $E = 45$ MeV/u according to CC calculations with the AMD densities (red solid lines). The one-step cross sections obtained by the DWBA calculation are also shown (blue dotted lines). The calculations are compared to the experimental data measured in inverse kinematics of ^{10}Be at 59.2 MeV/u [85], ^{12}Be at 55 MeV/u [86], and ^{10}C at 45.3 MeV/u [7].

model. For a further detailed discussion of the transition densities, higher quality data are necessary

D. Discussions

We discuss how the inelastic proton scattering cross sections can be linked with the neutron transition matrix element M_n of the $0_1^+ \to 2_1^+$ transition. The experimental studies of Refs. [3,9] discussed the neutron matrix elements of ^{12}Be and ^{16}C via a reaction analysis of the proton scattering data and concluded that there was a significant neutron contribution in the $0_1^+ \to 2_1^+$ transition. According to the model analysis in Refs. [3,9] using the Bernstein prescription [1], $B^{(n)}_{\lambda=2} = 17$ fm^4 of ^{12}Be was obtained via a reaction analysis using $B(E2) = 14.2(2.8)\ e^2$ fm^4, and $B^{(n)}_{\lambda=2} = 25$ fm^4 of ^{16}C was reduced using the updated data of $B(E2) = 2.6(9)\ e^2$ fm^4 [9]. The value of ^{16}C is consistent with our value of $B^{(n)}_{\lambda=2} = 27.0$ fm^4; however, the value of ^{12}Be is much smaller than the $B^{(n)}_{\lambda=2} = 51.1$ fm^4 found in the present calculation. In a theoretical study of proton scattering of ^{12}Be with an MCC calculation using the same AMD densities [11], a slightly smaller value $B^{(n)}_{\lambda=2} = 37$ fm^4 was used to reproduce the inelastic cross sections.

Reaction analyses with the Bernstein prescription usually assume the simple collective model transition densities given by the derivative of the matter density, and follows the relation of inelastic hadron (h, h') scattering cross sections with the

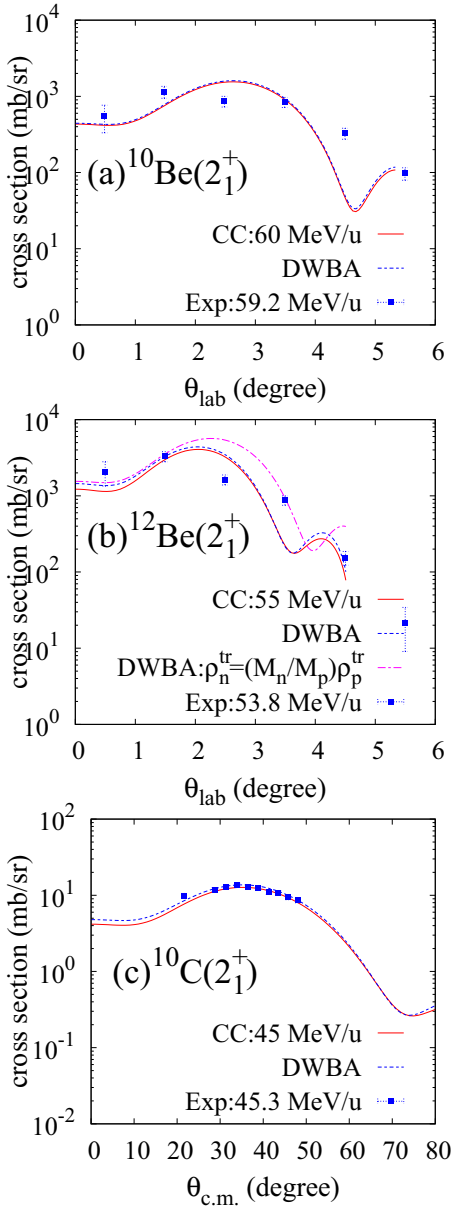

FIG. 11. Cross sections of inelastic proton scattering to the 2^+_1 state of (a) ^{10}Be at $E = 60$ MeV/u, (b) ^{12}Be at $E = 55$ MeV/u, and (c) ^{10}C at $E = 45$ MeV/u according to CC calculations (red solid lines). The one-step cross sections obtained by the DWBA calculation are also shown (blue dotted lines). In panel (b) for ^{12}Be, the DWBA calculation using the neutron transition density $\rho^{tr}_n(r) = (M_n/M_p)\rho^{tr}_p(r)$ is also shown for comparison (the magenta dash-dotted line). The calculations are compared to the experimental data measured in inverse kinematics of ^{10}Be at 59.2 MeV/u [3], ^{12}Be at 53.8 MeV/u [3], and ^{10}C at 45.3 MeV/u [7]. For the inelastic scattering of ^{10}Be(^{12}Be), θ_{lab} is kinematically limited within 5.6 (4.7) degrees; however, the data contain effects due to the finite size and angular spread of the incident beam, multiple scatterings in the target, and the detector geometry.

transition matrix elements such that

$$\sigma(h,h') \propto \left| b_n^{(h,h')} M_n + b_p^{(h,h')} M_p \right|^2, \tag{4}$$

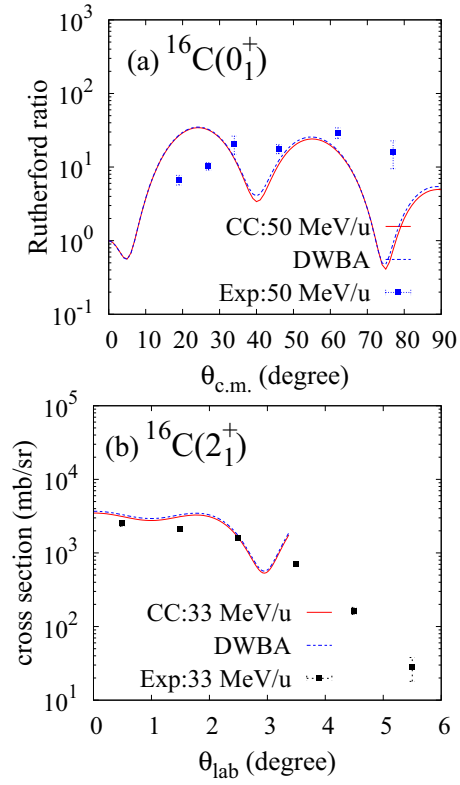

FIG. 12. (a) Cross sections of elastic proton scattering off ^{16}C at $E = 50$ MeV/u and (b) those of inelastic scattering at $E = 33$ MeV/u according to CC calculations with the AMD densities (red solid lines). The one-step cross sections obtained via the DWBA calculation are also shown (blue dotted lines). The calculations are compared to the experimental data [9,87] measured in inverse kinematics. For the inelastic scattering, θ_{lab} is kinematically limited within 3.6 degrees; however, the data contain effects due to the finite size and angular spread of the incident beam, multiple scatterings in the target, and the detector geometry.

where $b_n^{(h,h')}$ and $b_p^{(h,h')}$ are the neutron and proton field strengths of the external field from the hadron probe. For proton scattering, $b_n^{(p,p')}/b_p^{(p,p')}$ depends on the energy. A standard value of $b_n^{(p,p')}/b_p^{(p,p')} \approx 3$ at $E = 10$–50 MeV/u obtained from the data of various ordinary nuclei, is often used. The Bernstein prescription has been widely used for inelastic proton scattering; however, it relies heavily on the reaction model, which contains ambiguities such as the proton-nucleus optical potentials and the transition densities. The ansatz of Eq. (4) indicates the linear relationship of the squared cross section with the neutron (M_n) and proton (M_p) transition matrix elements. The ratio $b_n^{(p,p')}/b_p^{(p,p')}$ indicates the sensitivity of the cross sections to the neutron transition matrix element (M_n) relative to the proton transition matrix element (M_p) and is supposed to be system independent. This linear relationship may only be valid if the relation $\rho^{tr}_n(r) \propto \rho^{tr}_p(r)$ is satisfied.

However, this is not the case with ^{12}Be and ^{16}C, for which the neutron transition density has an outer amplitude compared to the proton transition density. Such an exotic neutron transition density behavior may have nontrivial

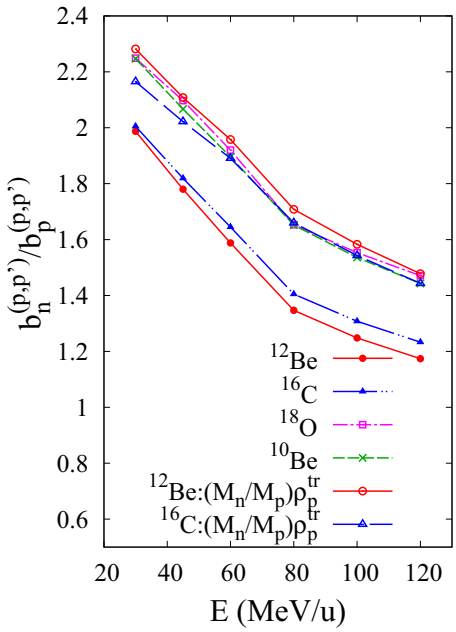

FIG. 13. $b_n^{(p,p')}/b_p^{(p,p')}$ ratio of the proton scattering at $E = 30$, 45, 60, 80, 100, and 120 MeV/u. The values for ^{18}O (magenta open squares), ^{10}Be (green crosses), ^{12}Be (red filled circles), and ^{16}C (blue filled triangles) were calculated with the default densities, and the values for ^{12}Be (red open circles), and ^{16}C (blue open triangles) for the $\rho_n^{tr}(r) = (M_n/M_p)\rho_p^{tr}(r)$ case are shown.

effects on the relationship between the cross sections and the transition matrix elements (M_n and M_p). To see these effects, we microscopically derive the ratio $b_n^{(p,p')}/b_p^{(p,p')}$ within the present MCC approach and discuss how the sensitivity of the cross section to M_n changes depending on the system as well as on the incident energy.

Here we assume that the AMD calculation gives the correct r dependence of $\rho_n^{tr}(r)$ and $\rho_p^{tr}(r)$ but contains ambiguity for the overall factor in each of the neutron and proton parts. By artificially changing the overall factor of $\rho_n^{tr}(r)$ or $\rho_p^{tr}(r)$, we can calculate the integrated cross sections and reduce the coefficients in the relation

$$\sigma(p, p') = \left|a_n^{(p,p')}({}^A Z, E)M_n + a_p^{(p,p')}({}^A Z, E)M_p\right|^2. \quad (5)$$

Here $a_n^{(p,p')}$ and $a_p^{(p,p')}$ are the system- and energy-dependent parameters determined from the calculated cross sections. The ratio $a_n^{(p,p')}/a_p^{(p,p')}$ is nothing but the ratio $b_n^{(p,p')}/b_p^{(p,p')}$ to be discussed.

In Fig. 13, we show the obtained result of $b_n^{(p,p')}/b_p^{(p,p')} = a_n^{(p,p')}/a_p^{(p,p')}$ for each system, ^{18}O, ^{10}Be, ^{12}Be, and ^{16}C, with the default transition densities depicted by open squares, crosses, filled circles, and filled triangles, respectively. For ^{12}Be and ^{16}C, we also show the result for the naive case of $\rho_n^{tr}(r) \propto \rho_p^{tr}(r)$ depicted by open circles and triangles, respectively, which were via the MCC calculation using $\rho_n^{tr}(r) = (M_n/M_p)\rho_p^{tr}(r)$. In all cases, the calculated values of $b_n^{(p,p')}/b_p^{(p,p')}$ show a similar energy dependence, i.e., decreasing with increasing E. This energy dependence primarily arises from the energy dependence of the effective g-matrix NN interactions. In fact, if the nucleon-nucleus optical potentials fixed at $E = 60$ MeV/u is used, $b_n^{(p,p')}/b_p^{(p,p')}$ varies slightly from 1.90 (1.64) to 1.89 (1.57) in the energy range of 30–120 MeV/u for proton scattering off ^{10}Be (^{12}Be).

At each energy, nearly the same values of $b_n^{(p,p')}/b_p^{(p,p')}$ are obtained for ^{18}O and ^{10}Be. In the calculation using the $\rho_n^{tr}(r) = (M_n/M_p)\rho_p^{tr}(r)$ assumption for ^{12}Be and ^{16}C, we obtained almost the same values as ^{18}O and ^{10}Be. These values can be regarded as standard values for ordinary systems with $\rho_n^{tr}(r) \approx (M_n/M_p)\rho_p^{tr}(r)$. However, in the exotic case $\rho_n^{tr}(r) \neq (M_n/M_p)\rho_p^{tr}(r)$ of ^{12}Be and ^{16}C with the default transition densities, the values of $b_n^{(p,p')}/b_p^{(p,p')}$ deviate significantly from the standard values: they are smaller than the standard values by approximately 0.3, indicating that the sensitivity of the cross sections to M_n is approximately 15% weaker than in the ordinary case of $\rho_n^{tr}(r) = (M_n/M_p)\rho_p^{tr}(r)$. The reason for the weaker sensitivity of the cross sections is that the outer amplitude of the neutron transition density significantly contributes to M_n but does not contribute much to the cross sections.

This result may suggest a possible modification to phenomenological reaction analyses. For simplicity, let us suppose that there is no ambiguity in the reaction model except for the neutron transition density $\rho_n^{tr}(r)$ and that other inputs are so reliable that the model can properly reproduce the cross sections for the ordinary case. If one performs an inconsistent analysis using $\rho_n^{tr}(r) = (M_n/M_p)\rho_p^{tr}(r)$ for the exotic case, one could extract an underestimated value of M_n from the observed cross sections.

V. SUMMARY

We investigated proton inelastic scattering off ^{18}O, ^{10}Be, ^{12}Be, and ^{16}C to the 2_1^+ states with a MCC calculation. The proton-nucleus potentials are microscopically derived by folding the Melbourne g-matrix NN interaction with the AMD densities of the target nuclei. The calculated result reasonably reproduces the elastic and inelastic proton scattering cross sections, and supports the dominant neutron contribution in the 2_1^+ excitation of ^{12}Be and ^{16}C.

The sensitivity of the inelastic scattering cross sections to the neutron transition density was discussed. Particular attention was paid to exotic systems such as ^{12}Be and ^{16}C in which the neutron transition density has a remarkable amplitude in the outer region compared to the proton transition density. This outer amplitude of the neutron transition density significantly contributes to the neutron matrix element M_n. However, its contribution to the inelastic cross sections is quite modest because the reaction process considered does not have a strong selectivity for the outer region. This result indicates that the Bernstein prescription is not valid in the case that the neutron transition density has an outer amplitude compared to the proton transition density. For such the exotic systems, a phenomenological analysis with a simple ansatz of the same transition densities for protons and neutrons tends to underestimate M_n.

The reaction model adopted here relies on MST with the g-matrix approximation to the nucleon-nucleon effective interaction, which becomes inadequate at low energies in general. Nevertheless, this framework appears to work quite well even near 25 MeV/nucleon, which is consistent with the result in Ref. [43]. To investigate the structure and reaction properties of unstable nuclei in detail, however, a more precise description of the reaction system will be necessary. The explicit treatment of rearrangement channels will be important at lower energies.

ACKNOWLEDGMENTS

The computational calculations of this work were performed by using the supercomputer in the Yukawa Institute for Theoretical Physics, Kyoto University. This work was partly supported by Grants-in-Aid of the Japan Society for the Promotion of Science (Grants No. JP18K03617, No. JP16K05352, and No. 18H05407) and by the grant for the RCNP joint research project.

APPENDIX: RESUMMATION FACTOR IN THE FOLDING MODEL CALCULATION

According to the multiple scattering theory for nucleon-nucleus scattering constructed by Kerman, McManus, and Thaler [49], the transition matrix T is given by

$$T = \frac{A}{A-1}T', \tag{A1}$$

where A is the mass number of the nucleus and T' is the transition matrix corresponding to the Schrödinger equation

$$\left[K + h + \frac{A-1}{A}\sum_{j=1}^{A}\tau_j - E\right]\Psi = 0, \tag{A2}$$

where K is the kinetic energy operator, h is the internal Hamiltonian of the nucleus, E is the total energy, and Ψ is the total wave function. τ_j is the effective interaction between the incident nucleon and a nucleon inside the nucleus, which is approximated to the Melbourne g-matrix NN interaction in this study. The two factors, $A/(A-1)$ in Eq. (A1) and $(A-1)/A$ in Eq. (A2), appear as a result of the *resummation* of the NN collisions originally written in terms of a bare NN interaction. Even though these resummation factors usually do not play a role, for nucleon scattering off a light nucleus especially at low energies, these factors may slightly modify the result as shown in Ref. [43]. These factors are taken into account in all the calculations shown in the present paper.

[1] A. M. Bernstein, V. R. Brown, and V. A. Madsen, Phys. Lett. B **103**, 255 (1981).
[2] Y. Kanada-En'yo and H. Horiuchi, Phys. Rev. C **55**, 2860 (1997).
[3] H. Iwasaki *et al.*, Phys. Lett. B **481**, 7 (2000).
[4] Y. Kanada-En'yo, Phys. Rev. C **71**, 014310 (2005).
[5] Y. Kanada-En'yo, Phys. Rev. C **71**, 014303 (2005).
[6] H. Sagawa, X. R. Zhou, X. Z. Zhang, and T. Suzuki, Phys. Rev. C **70**, 054316 (2004).
[7] C. Jouanne *et al.*, Phys. Rev. C **72**, 014308 (2005).
[8] M. Takashina, Y. Kanada-En'yo, and Y. Sakuragi, Phys. Rev. C **71**, 054602 (2005).
[9] H. J. Ong *et al.*, Phys. Rev. C **73**, 024610 (2006).
[10] T. J. Burvenich, W. Greiner, L. Guo, P. Klupfel, and P. G. Reinhard, J. Phys. G **35**, 025103 (2008).
[11] M. Takashina and Y. Kanada-En'yo, Phys. Rev. C **77**, 014604 (2008).
[12] Z. Elekes, N. Aoi, Z. Dombradi, Z. Fulop, T. Motobayashi, and H. Sakurai, Phys. Rev. C **78**, 027301 (2008).
[13] M. Wiedeking *et al.*, Phys. Rev. Lett. **100**, 152501 (2008).
[14] J. M. Yao, J. Meng, P. Ring, Z. X. Li, Z. P. Li, and K. Hagino, Phys. Rev. C **84**, 024306 (2011).
[15] C. Forssén, R. Roth and P. Navrátil, J. Phys. G **40**, 055105 (2013).
[16] A. M. Bernstein, V. R. Brown, and V. A. Madsen, Phys. Lett. B **71**, 48 (1977).
[17] S. Iversen *et al.*, Phys. Rev. Lett. **40**, 17 (1978).
[18] P. Grabmayr, J. Rapaport, and R. W. Finlay, Nucl. Phys. A **350**, 167 (1980).
[19] J. Kelly *et al.*, Phys. Lett. B **169**, 157 (1986).
[20] A. M. Bernstein, V. R. Brown, and V. A. Madsen, Phys. Rev. Lett. **42**, 425 (1979).
[21] E. Khan *et al.*, Phys. Lett. B **490**, 45 (2000).
[22] J. K. Jewell *et al.*, Phys. Lett. B **454**, 181 (1999).
[23] E. Khan *et al.*, Nucl. Phys. A **694**, 103 (2001).
[24] H. Scheit *et al.*, Phys. Rev. C **63**, 014604 (2000).
[25] E. Becheva *et al.*, Phys. Rev. Lett. **96**, 012501 (2006).
[26] C. M. Campbell *et al.*, Phys. Lett. B **652**, 169 (2007).
[27] Z. Elekes *et al.*, Phys. Rev. C **79**, 011302(R) (2009).
[28] N. Aoi *et al.*, Phys. Lett. B **692**, 302 (2010).
[29] S. Michimasa *et al.*, Phys. Rev. C **89**, 054307 (2014).
[30] L. A. Riley *et al.*, Phys. Rev. C **90**, 011305(R) (2014).
[31] A. Corsi *et al.*, Phys. Lett. B **743**, 451 (2015).
[32] M. L. Cortés *et al.*, Phys. Rev. C **97**, 044315 (2018).
[33] P. Navrátil, S. Quaglioni, G. Hupin, C. Romero-Redondo, and A. Calci, Phys. Scr. **91**, 053002 (2016).
[34] A. Idini, C. Barbieri, and P. Navrátil, Phys. Rev. Lett. **123**, 092501 (2019).
[35] K. Amos, P. J. Dortmans, H. V. von Geramb, S. Karataglidis, and J. Raynal, Adv. Nucl. Phys. **25**, 275 (2000).
[36] S. Karataglidis, Y. J. Kim, and K. Amos, Nucl. Phys. A **793**, 40 (2007).
[37] G. Bertsch, J. Borysowicz, H. McManus, and W. G. Love, Nucl. Phys. A **284**, 399 (1977).
[38] M. E.-A. Farid and G. R. Satchler, Nucl. Phys. A **438**, 525 (1985).
[39] D. T. Khoa, G. R. Satchler, and W. von Oertzen, Phys. Rev. C **56**, 954 (1997).
[40] K. Minomo, K. Ogata, M. Kohno, Y. R. Shimizu, and M. Yahiro, J. Phys. G **37**, 085011 (2010).

[41] M. Toyokawa, K. Minomo, and M. Yahiro, Phys. Rev. C **88**, 054602 (2013).
[42] M. Toyokawa, M. Yahiro, T. Matsumoto, K. Minomo, K. Ogata and M. Kohno, Phys. Rev. C **92**, 024618 (2015); **96**, 059905(E) (2017).
[43] K. Minomo, K. Washiyama, and K. Ogata, arXiv:1712.10121.
[44] K. Egashira, K. Minomo, M. Toyokawa, T. Matsumoto, and M. Yahiro, Phys. Rev. C **89**, 064611 (2014).
[45] K. Minomo and K. Ogata, Phys. Rev. C **93**, 051601(R) (2016).
[46] Y. Kanada-En'yo and K. Ogata, Phys. Rev. C **99**, 064601 (2019).
[47] Y. Kanada-En'yo and K. Ogata, Phys. Rev. C **99**, 064608 (2019).
[48] W. Haider, S. Rafi, J. R. Rook, and Y. K. Gambhir, Phys. Rev. C **93**, 054615 (2016).
[49] A. K. Kerman, H. McManus, and R. M. Thaler, Ann. Phys. (NY) **8**, 551 (1959).
[50] Y. Kanada-En'yo, H. Horiuchi, and A. Ono, Phys. Rev. C **52**, 628 (1995).
[51] Y. Kanada-En'yo and H. Horiuchi, Phys. Rev. C **52**, 647 (1995).
[52] Y. Kanada-En'yo, M. Kimura, and A. Ono, Prog. Theor. Exp. Phys. **2012**, 01A202 (2012).
[53] Y. Kanada-En'yo, H. Horiuchi, and A. Dote, Phys. Rev. C **60**, 064304 (1999).
[54] Y. Kanada-En'yo and H. Horiuchi, Phys. Rev. C **68**, 014319 (2003).
[55] Y. Kanada-En'yo and Y. Shikata, Phys. Rev. C **100**, 014301 (2019).
[56] R. Machleidt, K. Holinde, and Ch. Elster, Phys. Rep. **149**, 1 (1987).
[57] F. A. Brieva and J. R. Rook, Nucl. Phys. A **291**, 299 (1977).
[58] F. A. Brieva and J. R. Rook, Nucl. Phys. A **291**, 317 (1977).
[59] F. A. Brieva and J. R. Rook, Nucl. Phys. A **297**, 206 (1978).
[60] K. Hagino, T. Takehi, and N. Takigawa, Phys. Rev. C **74**, 037601 (2006).
[61] M. Kamimura, Nucl. Phys. A **351**, 456 (1981).
[62] J. P. Jeukenne, A. Lejeune, and C. Mahaux, Phys. Rev. C **16**, 80 (1977).
[63] T. Matsumoto, D. Ichinkhorloo, Y. Hirabayashi, K. Katō, and S. Chiba, Phys. Rev. C **83**, 064611 (2011).
[64] D. Ichinkhorloo, Y. Hirabayashi, K. Katō, M. Aikawa, T. Matsumoto, and S. Chiba, Phys. Rev. C **86**, 064604 (2012).
[65] H. Guo, Y. Watanabe, T. Matsumoto, K. Nagaoka, K. Ogata, and M. Yahiro, Phys. Rev. C **99**, 034602 (2019).
[66] T. Matsumoto, J. Tanaka, and K. Ogata, arXiv:1711.07209.
[67] Y. Kanada-En'yo, Phys. Rev. Lett. **81**, 5291 (1998).
[68] Y. Kanada-En'yo, Prog. Theor. Phys. **117**, 655 (2007); **121**, 895(E) (2009).
[69] Y. Kanada-En'yo, Phys. Rev. C **93**, 054307 (2016).
[70] Y. Kanada-En'yo, Phys. Rev. C **96**, 034306 (2017).
[71] E. Fabrici, S. Micheletti, M. Pignanelli, F. G. Resmini, R. De Leo, G. D'Erasmo, and A. Pantaleo, Phys. Rev. C **21**, 844 (1980).
[72] M. Pignanelli, S. Micheletti, R. De Leo, S. Brandenburg, and M. N. Harakeh, Phys. Rev. C **33**, 40 (1986).
[73] W. Bauhoff *et al.*, Nucl. Phys. A **410**, 180 (1983).
[74] S. Kato *et al.*, Phys. Rev. C **31**, 1616 (1985).
[75] S. Kato *et al.*, Nucl. Instrum. Methods **169**, 589 (1980).
[76] J. Kelly *et al.*, Phys. Rev. Lett. **45**, 2012 (1980).
[77] H. Ohnuma *et al.*, Nucl. Phys. A **514**, 273 (1990).
[78] D. R. Tilley, H. R. Weller, and C. M. Cheves, Nucl. Phys. A **564**, 1 (1993).
[79] D. R. Tilley, H. R. Weller, C. M. Cheves, and R. M. Chasteler, Nucl. Phys. A **595**, 1 (1995).
[80] D. R. Tilley, J. H. Kelley, J. L. Godwin, D. J. Millener, J. E. Purcell, C. G. Sheu, and H. R. Weller, Nucl. Phys. A **745**, 155 (2004).
[81] J. H. Kelley, J. E. Purcell, and C. G. Sheu, Nucl. Phys. A **968**, 71 (2017).
[82] H. J. Ong *et al.*, Phys. Rev. C **78**, 014308 (2008).
[83] B. E. Norum *et al.*, Phys. Rev. C **25**, 1778 (1982).
[84] J. L. Escudié, R. Lombard, M. Pignanelli, F. Resmini and A. Tarrats, Phys. Rev. C **10**, 1645 (1974); **11**, 639(E) (1975).
[85] M. D. Cortina-Gil *et al.*, Phys. Lett. B **401**, 9 (1997).
[86] A. A. Korsheninnikov *et al.*, Phys. Lett. B **343**, 53 (1995).
[87] L. Grassi *et al.*, J. Phys. Conf. Ser. **381**, 012088 (2012).
[88] T. Suzuki and T. Otsuka, Phys. Rev. C **56**, 847 (1997).
[89] A. Navin *et al.*, Phys. Rev. Lett. **85**, 266 (2000).
[90] S. D. Pain *et al.*, Phys. Rev. Lett. **96**, 032502 (2006).
[91] N. Imai *et al.*, Phys. Lett. B **673**, 179 (2009).
[92] R. Meharchand *et al.*, Phys. Rev. Lett. **108**, 122501 (2012).